

Mitigating boundary effects in finite temperature simulations of false vacuum decay

Kate Brown,^{1,*} Thomas P. Billam,^{2,†} and Ian G. Moss^{1,‡}

¹*School of Mathematics, Statistics and Physics,
Newcastle University, Newcastle upon Tyne, NE1 7RU, UK*

²*Joint Quantum Centre (JQC) Durham–Newcastle,
School of Mathematics, Statistics and Physics,
Newcastle University, Newcastle upon Tyne, NE1 7RU, UK*

(Dated: January 21, 2025)

Abstract

The physics of false vacuum decay during first-order phase transitions in the early universe may be studied in the laboratory via cold-atom analogue simulators. However, a key difference between analogue experiments and the early universe is the trap potential confining the atoms. Rapid seeded bubble nucleation has been shown to occur at the boundary of typical trap potentials, obscuring the bulk bubble nucleation rate. This difficulty must be overcome in order to reliably probe the bulk bubble nucleation rate in an analogue simulator experiment. In this paper we show that, at finite temperature, this deleterious boundary nucleation can be mitigated by adding a ‘trench’ to the potential, effectively screening the boundary with a region of higher atomic density. We show that this technique is effective in three different cold-atom analogue systems.

* kbrown97123@outlook.com

† thomas.billam@ncl.ac.uk

‡ ian.moss@ncl.ac.uk

I. INTRODUCTION

The universe underwent many phase transitions as it evolved through the early thermal plasma of the hot big bang, with the nature of its earliest transitions still an open question [1, 2]. Today, we may be able to observe signatures of a highly non-equilibrium history, in the form of cosmic strings [3], baryon asymmetry [4] and gravitational waves [5]. It is thus of interest to consider that some primordial phase transitions may have been first order, characterized by the universe supercooling into metastable “false vacuum” states and escaping via bubble nucleation.

The standard analytic treatment of bubble nucleation, established for first order phase transitions, and extended to vacuum decay in quantum field theory by Coleman et al. in the 1970s, seeks a semi-classical approximation to the field equations. The thermal and vacuum processes can be unified in the instanton approach, obtained by solving the relevant field equations in imaginary time [6, 7]. The instanton approximation constitutes a valuable resource for predicting decay rates in quantum field theory, although it does not provide a real-time picture of the decay process, or address vacuum bubble correlations [8]. Thus, the complementary approach of using an analogue system as a *quantum simulator* [9] to examine false vacuum decay in real time has gained traction in recent years [8, 10–22]. Ultracold atomic gases are a favored physical system with which to realize such analogues, owing to their ever-growing versatility and controllability, and were recently used to realize an analogue of thermally nucleated false vacuum decay in a ferromagnetic condensate [23]. Theoretically, such systems are amenable to stochastic numerical modelling under the general umbrella of stochastic classical field methods [24].

Unlike the early universe, cold-atom analogue systems are confined by traps, and so possess boundaries at which the atomic density falls to zero. Therefore, it is crucial to understand how false vacuum decay proceeds in the presence of these boundaries and to be able to create an analogue that reliably probes the bulk nucleation rate. While some previous works have investigated boundary effects in these analogues [14, 21], to our knowledge the latter has not been achieved. The main result of this paper is to show that, in a quasi-two-dimensional setup, boundary effects can be suppressed by incorporating a *trench* into a uniform ‘bucket’-type trapping potential [25] that screens the boundary of the trapping potential with a high-atomic-density region. Such a customised potential is likely realizable in quasi-two-dimensional geometries using digital micromirror device setups [26].

An extensively explored choice of cold-atom analogue is the pseudo-spin-1/2 setup of Fialko

et al. [10, 11]. This approach makes use of two spin states of an optically trapped spinor condensate, with these components coupled using a time-modulated microwave field. When averaged over long timescales and expressed in terms of the relative phase between components, the resultant description possesses the textbook vacuum-decay landscape; a quasi-relativistic real scalar effective field exhibiting a metastable local minimum (false vacuum) and a stable global minimum (true vacuum) separated by a potential barrier. This effective description has been examined in depth in one-dimensional periodic systems at both zero and finite temperature [8, 12, 13, 15–17, 19, 20, 22], with simulations reliably yielding bubbles in both regimes. However, the viability of this analogue hangs on the plausibility of overcoming a parametric instability present in the full time-dependent picture [15, 17, 19]. For this analogue, the potentially problematic seeding of rapid bubble nucleation at the trap boundary was noted in Ref. [14].

A second analogue, free from such parametric instabilities, has been experimentally realized using a ferromagnetic condensate consisting of two hyperfine levels of Sodium-23, with these components coupled by unmodulated microwave mixing [23]. In this analogue, the relative population imbalance between the components is the real scalar effective field exhibiting false and true vacua. Notably, Ref. [23] used a quasi-one-dimensional harmonic trapping potential; this setup has the advantage that boundary effects are not an issue since bubble nucleation is observed to primarily take place in the highest density region surrounding the trap minimum, but the disadvantage that the homogeneous bulk nucleation rate is not probed in an extended, constant-density region as it might be in an optical trap setup.

A third analogue, also free from parametric instabilities, can be found in a spin-1 gas with three occupied Zeeman levels coupled via unmodulated Raman and radio-frequency mixing [18, 21]. In this analogue, one of the two real relative phases between the components serves as the effective scalar field degree of freedom exhibiting false and true vacua. This lessercharted territory has thus far been explored for a one-dimensional zero-temperature system [18] and a two-dimensional finite-temperature system [21], the latter of which revealed the seeding of rapid bubble nucleation at the trap boundary. In particular, the inclusion of a simple square trapping potential in a quasi-two-dimensional (quasi-2D) gas, with parameters appropriate to a Lithium-7 system, was found to accelerate vacuum decay, with bubbles nucleating preferentially along the trap boundary to such an extent that a reliable measure of the bulk nucleation rate could not be isolated.

In this paper we generalize previous results on boundary nucleation, by applying the stochastic projected Gross–Pitaevskii (SPGPE) methodology to finite-temperature, quasi-2D analogues in

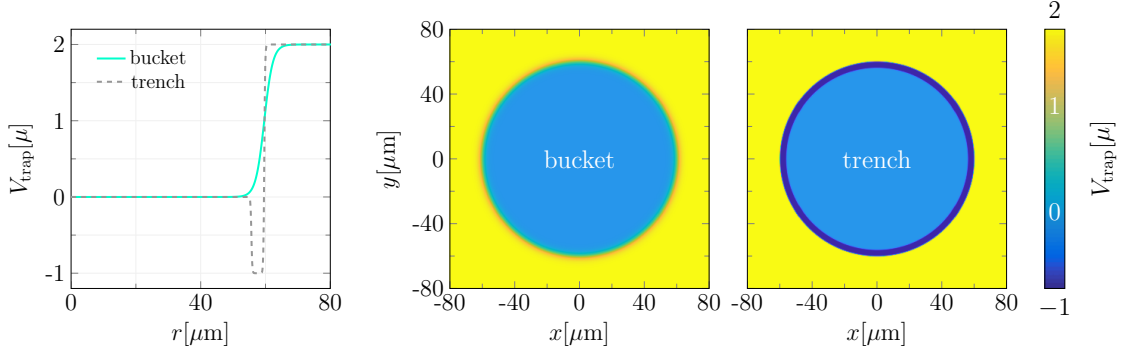


FIG. 1. The circular trapping potential V_{trap} given by Equation (7), shown for the Potassium-39 parameters listed in Table I. We examine two trap variations: a ‘bucket’ trap, where $r_a = r_b$, and a ‘trench’ trap, where $r_a < r_b$. Left: trapping potential as a function of radius. Right: The full spatial profile of each trapping potential.

which the atoms are confined in a circular optical ‘bucket’ trap¹, as shown in Figure 1. Rather than restrict our approach to a particular analogue, we investigate all three of the pseudo-spin-1/2, ferromagnetic, and spin-1 analogues described above. In a simple circular bucket trap, boundary nucleation is preferential to the extent that reliably measuring the bulk nucleation rate would be difficult in a system of any experimentally realistic size. However, we show that incorporating a *trench* near the edge of the trapping potential strongly suppresses boundary nucleation, allowing one to observe nucleation events in the bulk of a realistic-sized system; this constitutes a vital step towards realizing an analogue experiment that probes the bulk bubble nucleation rate.

The remainder of this paper is structured as follows. In Sections II–IV we present — in turn for the pseudo-spin-1/2, ferromagnetic, and spin-1 analogues — more details of the theoretical descriptions and parameters used in our simulations. Our simulation results use both pure ‘bucket’ traps and ‘bucket’ traps with the added ‘trench’. In each of these sections we conduct simulations using parameters suitable for realization of the analogue with a particular atomic species, respectively: Potassium-39, Sodium-23, and Rubidium-87. Section V comprises our conclusions.

¹ A circular ‘bucket’ is chosen to best avoid particularly rapid seeded nucleation at sharp corners, which we observed in our preliminary simulations.

II. PSEUDO-SPIN-1/2 ANALOGUE: POTASSIUM-39

The Potassium-39 system we consider here is similar to the one described in Ref [22]. It is based on potassium atoms occupying two Zeeman levels condensed in a two-dimensional optical ‘bucket’ trap. Atomic collisions between atoms in the same level, or different levels, are described by three scattering parameters $g_{\uparrow\uparrow}$, $g_{\downarrow\downarrow}$ and $g_{\uparrow\downarrow}$. In addition, a time-modulated microwave field provides mixing between the atoms in each level, described by a Rabi frequency Ω and a dimensionless modulation parameter λ . The time-averaged Hamiltonian is

$$H = \int \left\{ -\frac{\hbar^2}{2m} \psi^\dagger \nabla^2 \psi + \frac{1}{2} \sum_{i,j} g_{ij} |\psi_i|^2 |\psi_j|^2 + (V_T - \mu) \psi^\dagger \psi - \frac{\hbar\Omega}{2} \psi^\dagger \sigma_x \psi + \frac{\hbar\Omega}{2} g' (\psi^\dagger \sigma_y \psi)^2 \right\} dx dy. \quad (1)$$

The scattering parameters g_{ij} determine the relative number density of the two components in the ground state of the system, n_\uparrow and n_\downarrow , and $g' = \lambda^2/4\sqrt{n_\uparrow n_\downarrow}$. Important physical parameters are the frequency scale $\omega_m = (g_{\uparrow\uparrow} + g_{\downarrow\downarrow} - 2g_{\uparrow\downarrow})n/\hbar$ and healing length $\xi_m = (\hbar/m\omega_m)^{1/2}$, where $n = n_\uparrow + n_\downarrow$ is the total number density.

In the first configuration, the trapping potential $V_T(x, y)$ forms a circular ‘bucket’ trap. Outside the trap, the potential drives the density to zero. There is a narrow transition region at the edge of the trap, which we can arrange to have a width approximately equal to ξ_m . The bulk density inside the trap has a constant value n in the initial state. In the second configuration, a drop in potential, or trench, on the inner edge of the circular edge increases the condensate density there. Figure 1 shows these configurations.

In [22], it was shown that the system can be described by an effective theory for a single scalar field related to the relative phase φ of the two components. The canonically normalised field $\phi = v\varphi$, where

$$v^2 = n_\uparrow n_\downarrow \xi_m^2 \hbar \omega_m / n. \quad (2)$$

The field equation has Klein-Gordon form

$$c_\varphi^{-2} \ddot{\phi} - \nabla^2 \phi + \frac{dV}{d\phi} = 0, \quad (3)$$

where the sound speed $c_\varphi = \xi_m \omega_m (n_\uparrow n_\downarrow)^{1/2} \sqrt{2}/n$ and the potential

$$V(\phi) = \hbar\Omega \sqrt{n_\uparrow n_\downarrow} \left(-\cos \frac{\phi}{v} + \frac{1}{2} (\lambda^2 - 1) \sin^2 \frac{\phi}{v} \right). \quad (4)$$

When $\lambda^2 > 1$, the potential has a local minimum, or false vacuum, at $\phi = v\pi$ and a global minimum, or true vacuum, at $\phi = 0$. The energy density difference between the vacua is $\epsilon = 2\hbar\Omega \sqrt{n_\uparrow n_\downarrow}$.

For the finite temperature simulations, we solve the simple-growth variant of the stochastic, projected Gross-Pitaevski equation (SPGPE) for the condensate fields ψ_i [27–30]. The SPGPE is

$$i\hbar \frac{\partial \psi_i}{\partial t} = \mathcal{P} \left\{ (1 + i\gamma) \frac{\partial H}{\partial \psi_i} + \eta_i \right\}, \quad (5)$$

where H is the Hamiltonian, $i\gamma$ is a dissipation term and η_m is a Gaussian stochastic noise term with statistics

$$\langle \eta_i(\mathbf{r}, t) \eta_j^\dagger(\mathbf{r}', t') \rangle = \frac{2\gamma k_B T}{\hbar \omega_m n} \delta_{ij} \delta(\mathbf{r} - \mathbf{r}') \delta(t - t'). \quad (6)$$

The equation is solved in a two-dimensional periodic box containing the circular trap with functional form

$$V_{\text{trap}} = \frac{1}{2} \left[2\mu - \mu \tanh\left(\frac{r - r_a}{\sigma}\right) + 3\mu \tanh\left(\frac{r - r_b}{\sigma}\right), \right]. \quad (7)$$

For the pure ‘bucket’ trap we use $r_a = r_b = 59.6\mu\text{m}$ and $\sigma = 2.64\mu\text{m}$, whereas for the ‘trench’ trap we use $r_a = 55.6\mu\text{m}$, $r_b = 59.6\mu\text{m}$, and $\sigma = 0.264\mu\text{m}$. Averages of observables over many runs represent thermal ensemble averages. We make the conceptual leap that snapshots taken from individual runs are representative of what could be observed in a real experiment [24].

The system is initialized in the false vacuum state. This is achieved by equilibrating in the true vacuum state and subsequently changing the sign of the Rabi frequency Ω with a piecewise linear ramp, switching the true and false vacua [19]. Simulations have been run with a range of timings in the initialisation process to ensure robustness of the procedure. Times in the final results are expressed relative to the end of the ramp.

A sequence of three runs in the pure ‘bucket’ trap is shown in figure 2, for parameters in table I. These show that the bubbles nucleate preferentially on the walls of the trap. This phenomenon can be understood in terms of nucleation theory, as mentioned in section I. There is a critical size for bubbles of the true vacuum phases, such that smaller bubbles collapse and larger bubbles grow. The bubble nucleation rate is exponentially suppressed by the energy of the critical bubble. However, near to a boundary, it is possible to have a fraction of a bubble with a fraction of the energy, which has far less suppression. The simulations show that this fraction is approximately one half, as predicted in a recent paper on seeded nucleation of bubbles [4].

To observe bubbles nucleating inside the trap, rather than at the edges, we add a ‘trench’ in the potential. As described in section I, this screens the edge of the trap with a region of higher atomic density that acts like an anti-surfactant to prevent bubble nucleating at the edges. The sequence of runs in figure 3 shows the effect of having a trench in the potential. The potential has been chosen

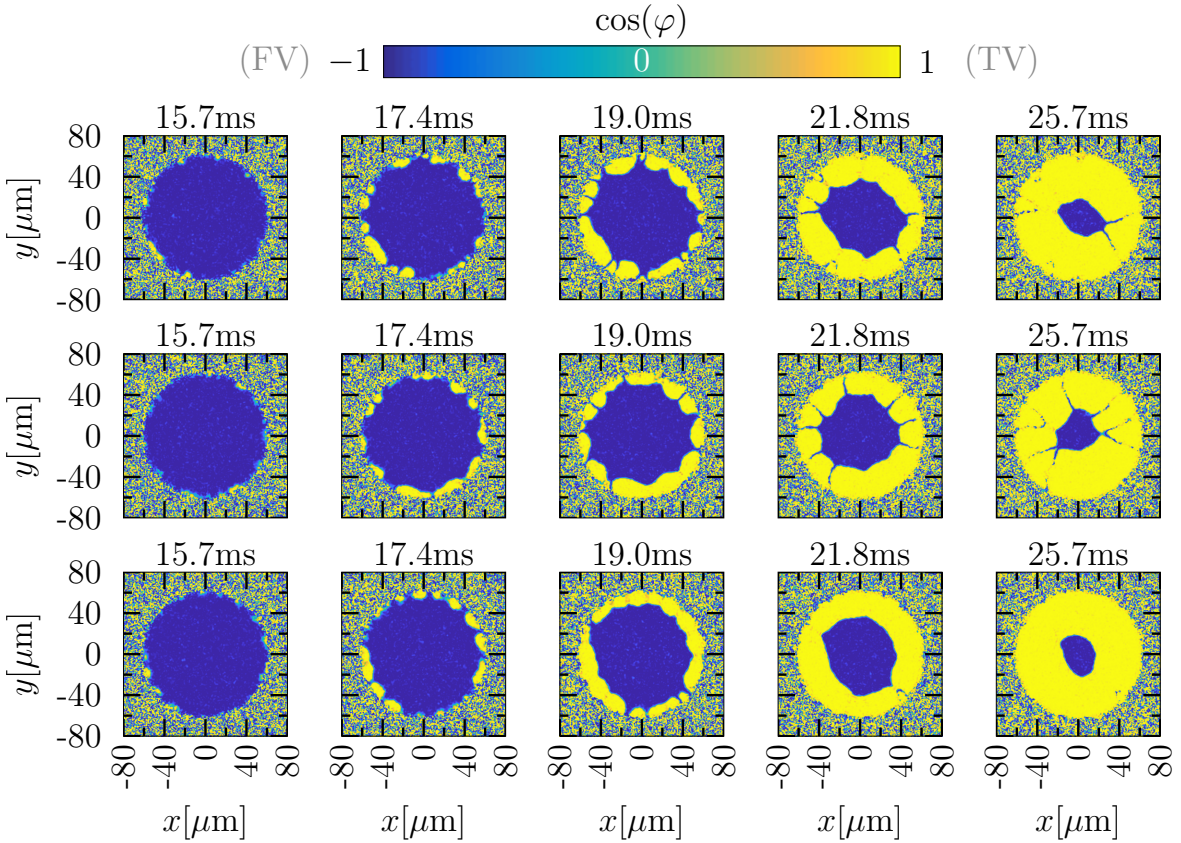


FIG. 2. The evolution of $\cos(\varphi)$ in a pseudo-spin-1/2 gas of Potassium-39 atoms confined to a circular ‘bucket’ potential at $T = 12.61\text{nK}$. Here $r_a = r_b = 59.6\mu\text{m}$ and $\sigma = 2.64\mu\text{m}$, with all relevant parameters listed in Table I. Each row of snapshots shows the progression of a unique simulation run, with time increasing from left to right. Identical parameters are used across realizations and all quantities are expressed in physical units.

so that the density inside the trench is twice the density inside the rest of the trap. We found that changing the shape of the trench, whilst maintaining its qualitative features, did not affect our conclusions.

III. FERROMAGNETIC ANALOGUE: SODIUM-23

Sodium-23 is the only BEC system so far with actual experimental results on bubble formation [23]. We will model a version of the system which is extended into two dimensions. The basic system has two hyperfine levels. In this case the frequency ω_m is negative. The microwave field mixing the levels is unmodulated, but is detuned by an amount δ from the frequency separation

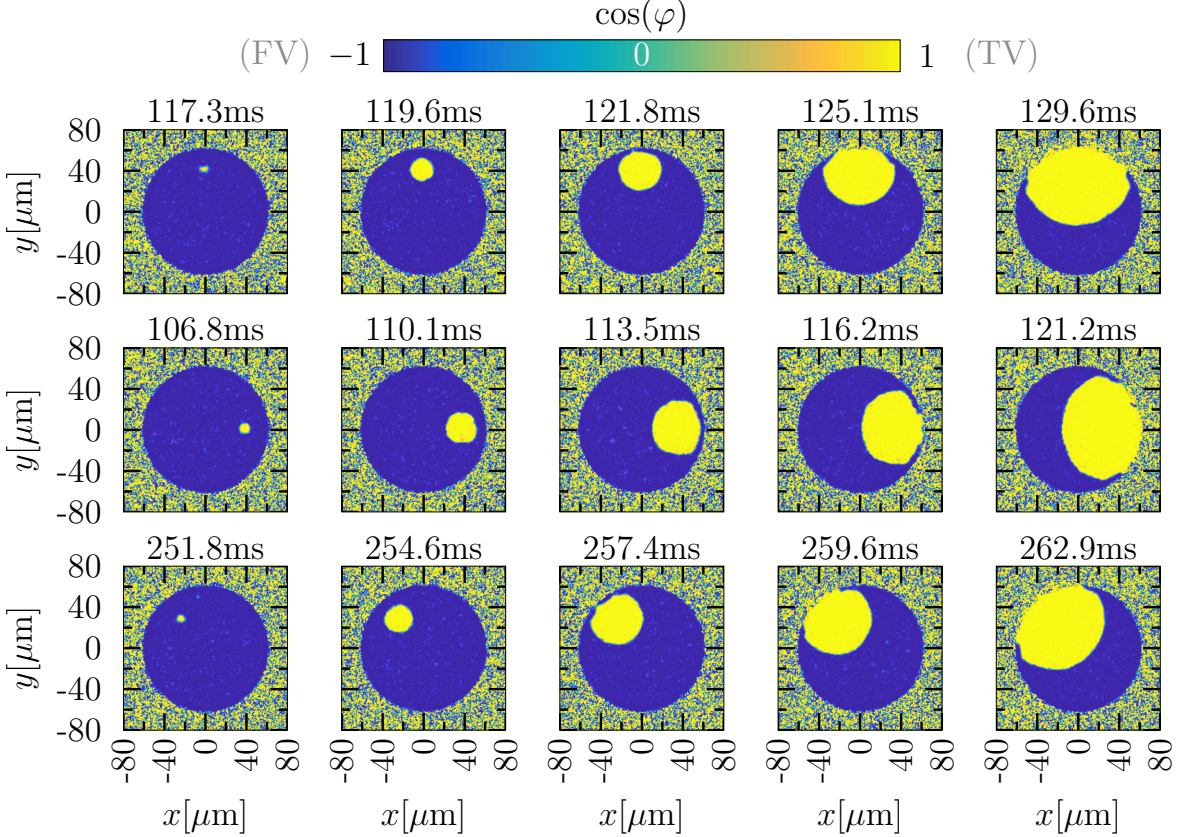


FIG. 3. The evolution of $\cos(\varphi)$ in a pseudo-spin-1/2 gas of Potassium-39 atoms confined to a ‘trench’ potential at $T = 12.61\text{nK}$. Here $r_a = 55.6\mu\text{m}$, $r_b = 59.6\mu\text{m}$, and $\sigma = 0.264\mu\text{m}$, with all relevant parameters listed in Table I. Each row of snapshots shows the progression of a unique simulation run, with time increasing from left to right. Identical parameters are used across realizations and all quantities are expressed in physical units.

between the two levels. The mean field Hamiltonian is

$$H = \int \left\{ -\frac{\hbar^2}{2m} \psi^\dagger \nabla^2 \psi + \frac{1}{2} \sum_{i,j} g_{ij} |\psi_i|^2 |\psi_j|^2 + (V_T - \mu) \psi^\dagger \psi - \frac{\hbar \Omega}{2} \psi^\dagger \sigma_x \psi + \frac{\hbar \delta}{2} \psi^\dagger \sigma_z \psi \right\} dx dy. \quad (8)$$

The effective theory is now in the magnetisation sector Z , where

$$Z = \frac{n_\uparrow - n_\downarrow}{n_\uparrow + n_\downarrow}. \quad (9)$$

The canonically normalised field is $\phi = (\hbar^2 n / 4m)^{1/2} \cos^{-1}(Z)$, with field equation

$$c_z^{-1} (c_z^{-1} \dot{\phi}) - \nabla^2 \phi + \frac{\partial V}{\partial \phi}. \quad (10)$$

The potential is

$$V(Z) = \frac{n}{4} \left(\hbar \omega_m Z^2 - 2\hbar \Omega \sqrt{1 - Z^2} - 2\hbar \delta Z \right). \quad (11)$$

TABLE I. Physical parameters used in the potassium-39 simulations.

Parameter	Value
number density	$n = 100 \mu\text{m}^{-2}$
magnetic field	$B = 57.5\text{G}$
Rabi frequency	$\Omega = 100 \times 2\pi\text{Hz}$
trap frequency	$\omega_{\perp} = 5 \times 2\pi\text{kHz}$
frequency scale	$\omega_m = 23.14\text{kHz}$
healing length	$\xi_m = 0.264\mu\text{m}$
temperature	$T_m = 48.5\text{nK}$

There is a critical value for the detuning δ_c at which the potential develops a false vacuum minimum.

In this model, the sound speed is dependent on Z ,

$$c_z = \sqrt{\frac{\hbar\Omega}{2m}}(1 - Z^2)^{-1/4}. \quad (12)$$

This field dependence in the sound speed breaks the Lorentz symmetry. This is not a significant issue for finite temperature nucleation, where Lorentz symmetry is broken in any case.

At zero temperature, it is undesirable for an analogue system describing elementary particle physics to break Lorentz invariance. However, the system has features that make it resemble one with Lorentz symmetry. Firstly, the nucleation of bubbles is very close to the Lorentz invariant case if the barrier is very narrow, and Z remains close to the false vacuum value inside the bubble instanton. Secondly, bubbles grow in a very similar way to the bubbles in a Lorentz invariant theory (shown in appendix A).

A sequence of three runs for the ‘bucket’ trap is shown in figure 4, for parameters in table II. The length parameters in the potential (r_a , r_b , and σ) are chosen to be the same relative to the healing length as they were in section II. These show that the bubbles nucleate preferentially on the walls of the trap. The runs also show an interesting feature of the sodium system that vortices can form between the bubbles. This is not restricted to the trap geometry, but is also seen in simulations of the sodium system in a periodic box.

The sequence of runs in figure 5 shows the effect of having the ‘trench’ in the potential. The details of the trench are the same as in the potassium system, and the trench again suppresses bubble nucleation at the boundary. It is also apparent that the bubbles in the bulk of the sodium

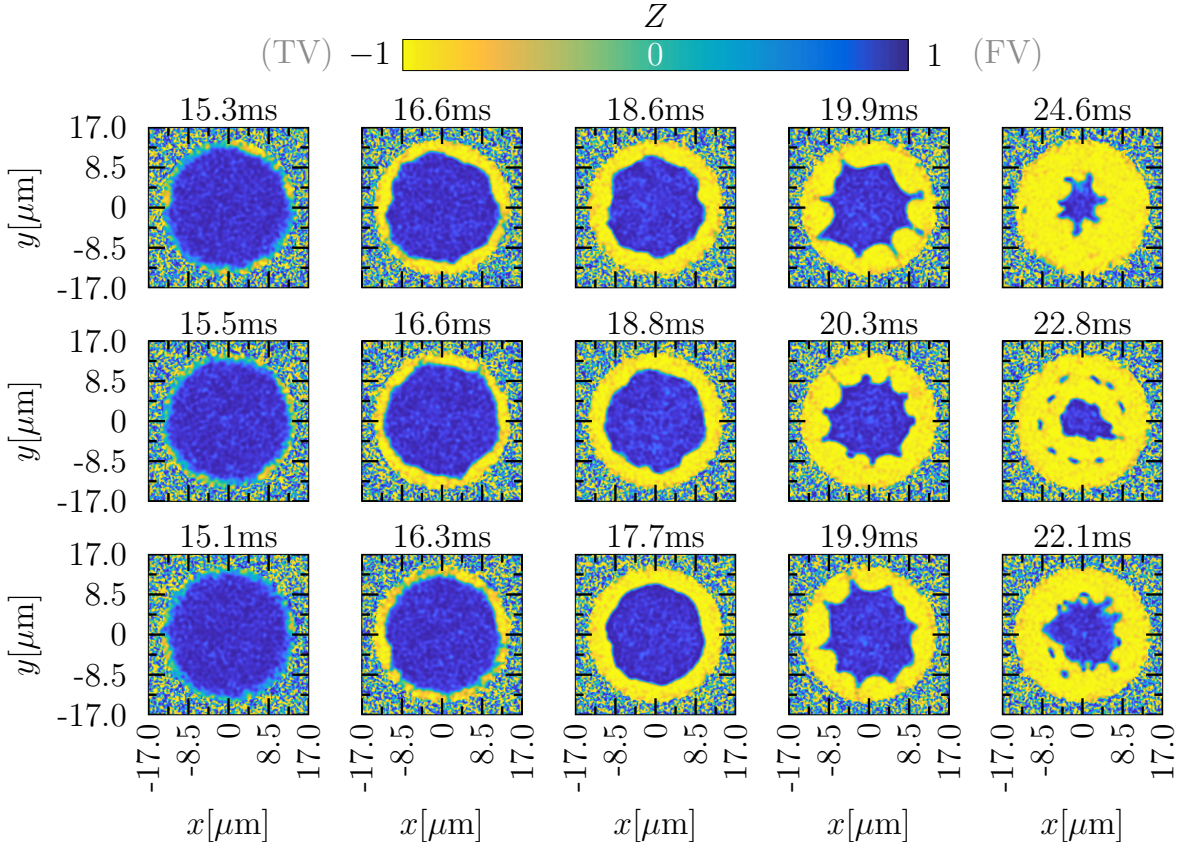


FIG. 4. The evolution of the magnetization, Z , in a pseudo-spin-1/2 gas of Sodium-23 atoms confined to a circular ‘bucket’ potential at $T = 68.08\text{nK}$. Here $r_a = r_b = 14.2\mu\text{m}$ and $\sigma = 1.42\mu\text{m}$, with all relevant parameters listed in Table II. Each row of snapshots shows the progression of a unique simulation run, with time increasing from left to right. Identical parameters are used across realizations and all quantities are expressed in physical units.

system become distorted quite early on in their growth phase. This is due to the bubble wall becoming thinner as the bubble expands, and the large spatial gradients in the wall cause the breakdown of the effective theory. This phenomenon is not restricted to the sodium system, and happens eventually to bubbles in all the analogue vacuum decay systems. In each system there is a small parameter that controls the validity of the effective theory. In the potassium-39 system of section II (and the rubidium-87 system to be considered in section IV) the parameter is Ω/ω_m , which can be tuned to be as small as we like, and was 0.008 in the potassium-39 simulations. In the sodium system, the parameter is fixed by the scattering lengths. If we define $\omega_n = (g_{\uparrow\uparrow} + g_{\downarrow\downarrow} + 2g_{\uparrow\downarrow})n/\hbar$, then the small parameter is $|\omega_m/\omega_n| = 0.04$.

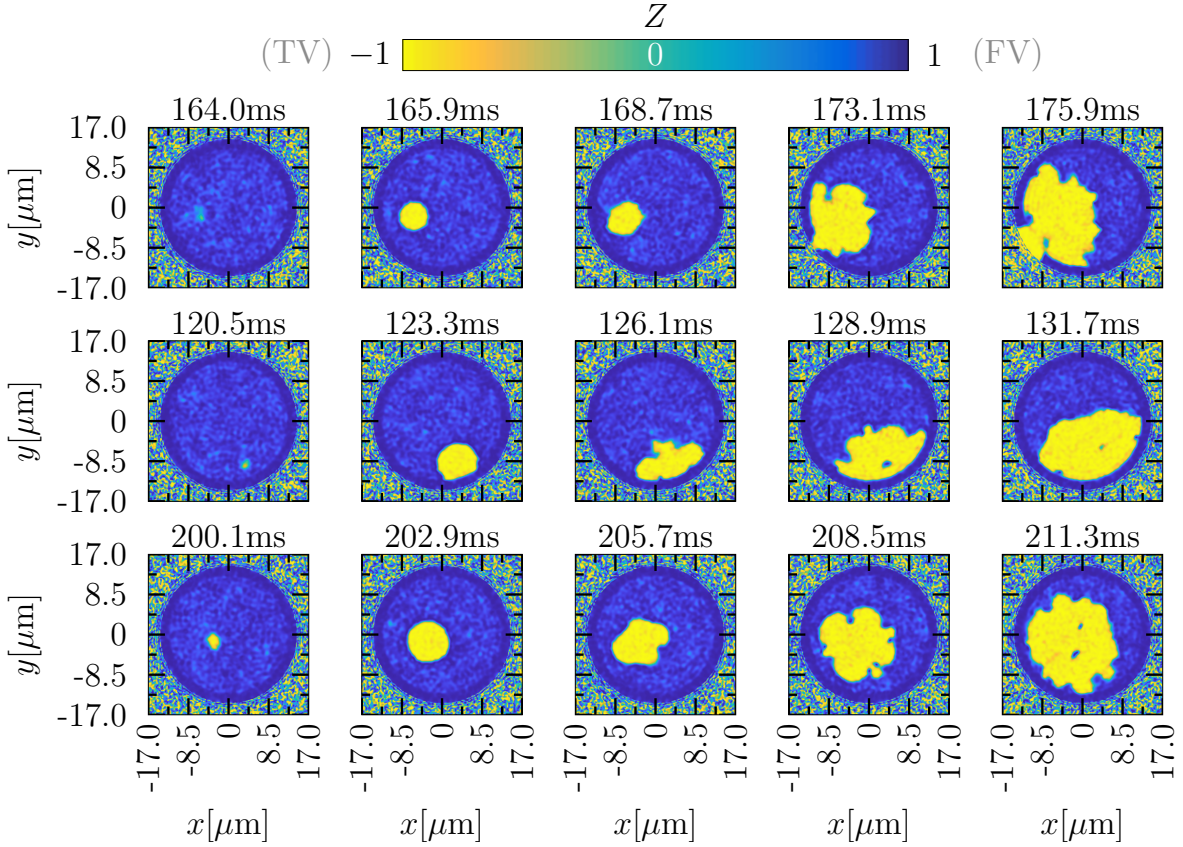


FIG. 5. The evolution of the magnetization, Z , in a pseudo-spin-1/2 gas of Sodium-23 atoms confined to a ‘trench’ potential at $T = 68.08\text{nK}$. Here $r_a = 12.8\mu\text{m}$, $r_b = 14.2\mu\text{m}$, and $\sigma = 0.142\mu\text{m}$, with all relevant parameters listed in Table II. Each row of snapshots shows the progression of a unique simulation run, with time increasing from left to right. Identical parameters are used across realizations and all quantities are expressed in physical units.

IV. SPIN-1 ANALOGUE: RUBIDIUM-87

The false vacuum decay proposal with Rubidium-87 uses a three level system, with populations n_+ , n_0 and n_- in $m = +1$, $m = 0$ and $m = -1$ Zeeman levels [18, 21]. The quadratic Zeeman effect, which plays an important role in determining the vacuum state of the system, is parameterised by a frequency ω_q . The coupling between the levels is parameterised by just two parameters g and g' , because of rotational symmetry. The microwave field mixing the levels is unmodulated, and an extra source of coupling between the levels is introduced using a Raman transition, parameterised by a constant λ , as shown in figure 6. We define the natural frequency of the system to be $\omega_m = gn$.

The Hamiltonian for the rubidium system, when expressed in terms of a three component mean

TABLE II. Physical parameters used in the sodium-23 simulations.

Parameter	Value
number density	$n = 500 \mu\text{m}^{-2}$
Rabi frequency	$\Omega = 100 \times 2\pi\text{Hz}$
detuning	$\delta - \delta_c = 17 \times 2\pi\text{Hz}$
trap frequency	$\omega_\perp = 12.5 \times 2\pi\text{kHz}$
frequency scale	$\omega_m = -80.18\text{kHz}$
healing length	$\xi_m = 0.142\mu\text{m}$
temperature	$T_m = 184\text{nK}$

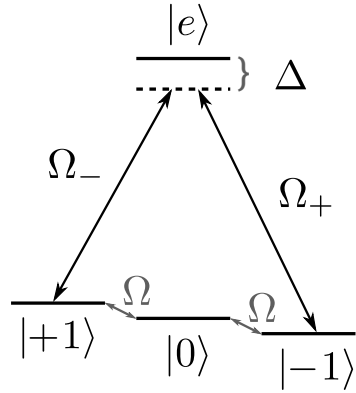


FIG. 6. Level coupling diagram for the spin-1 Rubidium-87 system. The $F = 1$ spin states, labeled $|m\rangle$, are coupled by a resonant RF beam with Rabi frequency Ω , and by a two-photon Raman coupling induced by off-resonant optical beams with Rabi frequencies Ω_{\pm} , zero two-photon detuning, and detuning Δ from the excited state $|e\rangle$

field ψ , is

$$H = \int \left\{ -\frac{\hbar^2}{2m} \psi^\dagger \nabla^2 \psi + (V_T - \mu) \psi^\dagger \psi + \mathcal{V} \right\} dx dy. \quad (13)$$

where the scattering and interaction terms are

$$\begin{aligned} \mathcal{V} = & \hbar \omega_q (\bar{\psi} J_z^2 \psi) + \frac{1}{2} g (\bar{\psi} \psi)^2 + \frac{1}{2} g' (\bar{\psi} \mathbf{J} \psi)^2 \\ & + \frac{1}{2} \hbar \Omega \bar{\psi} J_x \psi + -\frac{1}{8} \hbar \lambda^2 \bar{\psi} (J_+^2 + J_-^2) \psi. \end{aligned} \quad (14)$$

The 2D scattering coefficients are related to scattering lengths in the F channels a_0 and a_2 [31, 32]

$$g = \left(\frac{8\pi\hbar^3\omega_\perp}{m} \right)^{1/2} \frac{a_0 + 2a_2}{3}, \quad g' = \left(\frac{8\pi\hbar^3\omega_\perp}{m} \right)^{1/2} \frac{a_2 - a_0}{3}. \quad (15)$$

For rubidium-87, the ratio $g'/g = -0.00463$. The quadratic Zeeman energy

$$\hbar\omega_q = \frac{(g_F\mu_B B)^2}{\Delta E_{\text{hfs}}}, \quad (16)$$

where $g_F \approx 1/2$ and μ_B is the Bohr magneton. The Raman coupling coefficient λ was shown to be

$$\lambda^2 = \frac{\Omega_+ \Omega_+}{\Omega \Delta_e}. \quad (17)$$

where Ω is the RF Rabi frequency, Ω_\pm the optical Rabi frequency and Δ_e the detuning.

The state of lowest energy when $g' < 0$, $g > 0$ and $0 < \hbar\omega_q < -2g'n$ is called the broken axisymmetric (BA) phase, in which all three Zeeman levels are occupied. There is an effective theory for the relative phase φ of the $m = +1$ and $m = -1$ components of the BEC in the BA phase. The field equation has Klein-Gordon form (3) with potential

$$V = 2\hbar\Omega n_+ \left(\lambda_c^2 \cos \varphi + \frac{1}{2} \lambda^2 \sin^2 \varphi \right), \quad (18)$$

where

$$\lambda_c = \left(\frac{1 - \hbar\omega_q/2ng'}{1 + \hbar\omega_q/2ng'} \right)^{1/2}. \quad (19)$$

A sequence of three runs for the ‘bucket’ trap potential is shown in figure 7, for parameters in table III. Again, the length parameters in the potential are chosen the same relative to the healing length as they were in section II. These sequences show that the bubbles nucleate preferentially on the walls of the trap. The sequence of runs in figure 8 shows the effect of having the ‘trench’ in the potential, which again acts to suppress nucleation at the boundaries.

The small value of the ratio g'/g results in parameter choices for the rubidium system that are especially challenging. Parameter values for related systems using potassium-41 or lithium-7 have the potential to be more experimentally favorable, but this has to be offset by the ease of cooling rubidium-87 compared to these alternative species.

V. CONCLUSIONS

In order to gain insight into the physics of false vacuum decay in the early universe from a cold-atom analogue simulator, a key next step is to reliably probe experimentally the bulk bubble nucleation rate in a homogeneous condensate. In this paper we described three previously proposed analogue systems, and identified the previous issues with rapid bubble nucleation at the trap boundary that were identified in previous works. For the case of an optically-trapped system

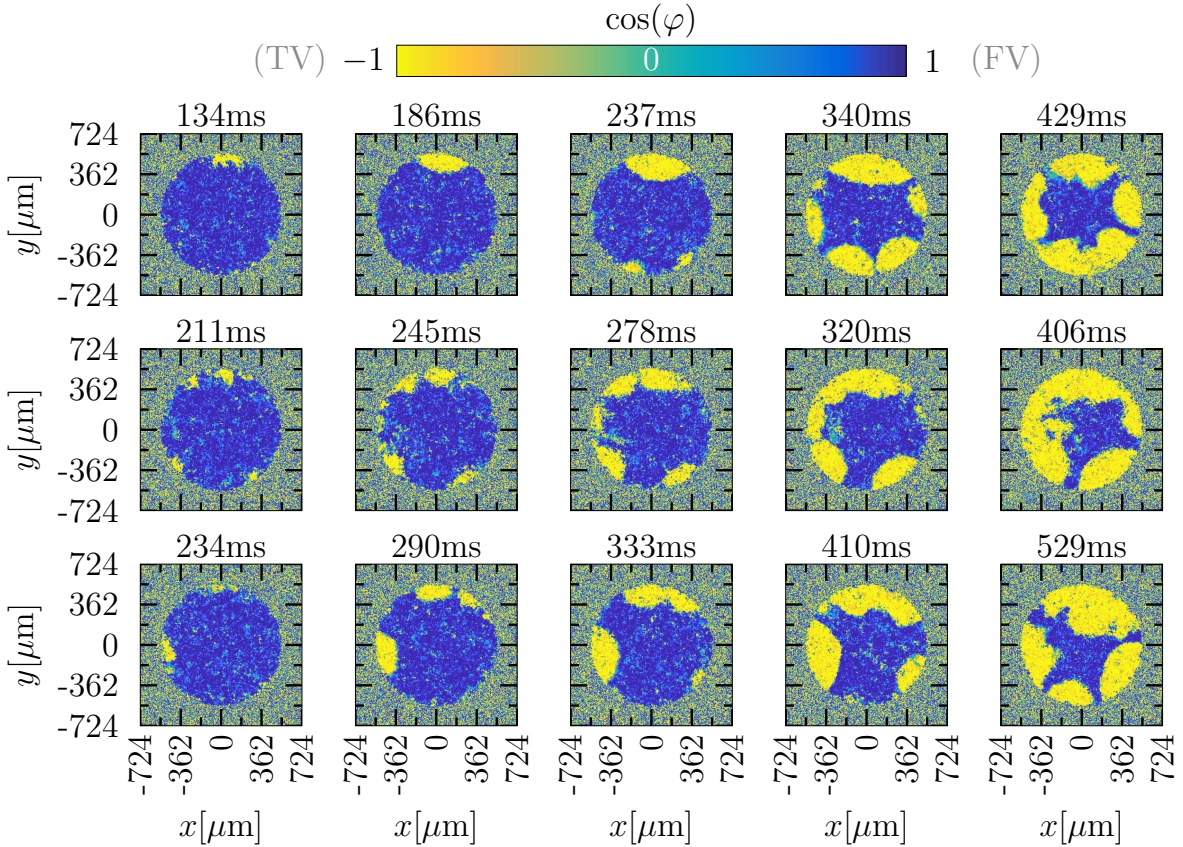


FIG. 7. The evolution of $\cos(\varphi)$ in a spin-1 gas of Rubidium-87 atoms confined to a circular ‘bucket’ potential at $T = 16.56\text{nK}$. Here $r_a = r_b = 543\mu\text{m}$ and $\sigma = 18.1\mu\text{m}$, with all relevant parameters listed in Table III. Each row of snapshots shows the progression of a unique simulation run, with time increasing from left to right. Identical parameters are used across realizations and all quantities are expressed in physical units.

at finite temperature our SPGPE simulations show that, in all three analogues, this deleterious boundary nucleation can be mitigated by adding a ‘trench’ to the potential, effectively screening the boundary with a region of higher atomic density than found in the uniform bulk of the system. Our results suggest that a potential with such a ‘trench’ — created, for example, using digital micromirror devices [26] — may allow forthcoming experiments to measure bulk bubble nucleation rates in realistically sized systems.

Data supporting this publication are openly available under a Creative Commons CC-BY-4.0 License in [33].

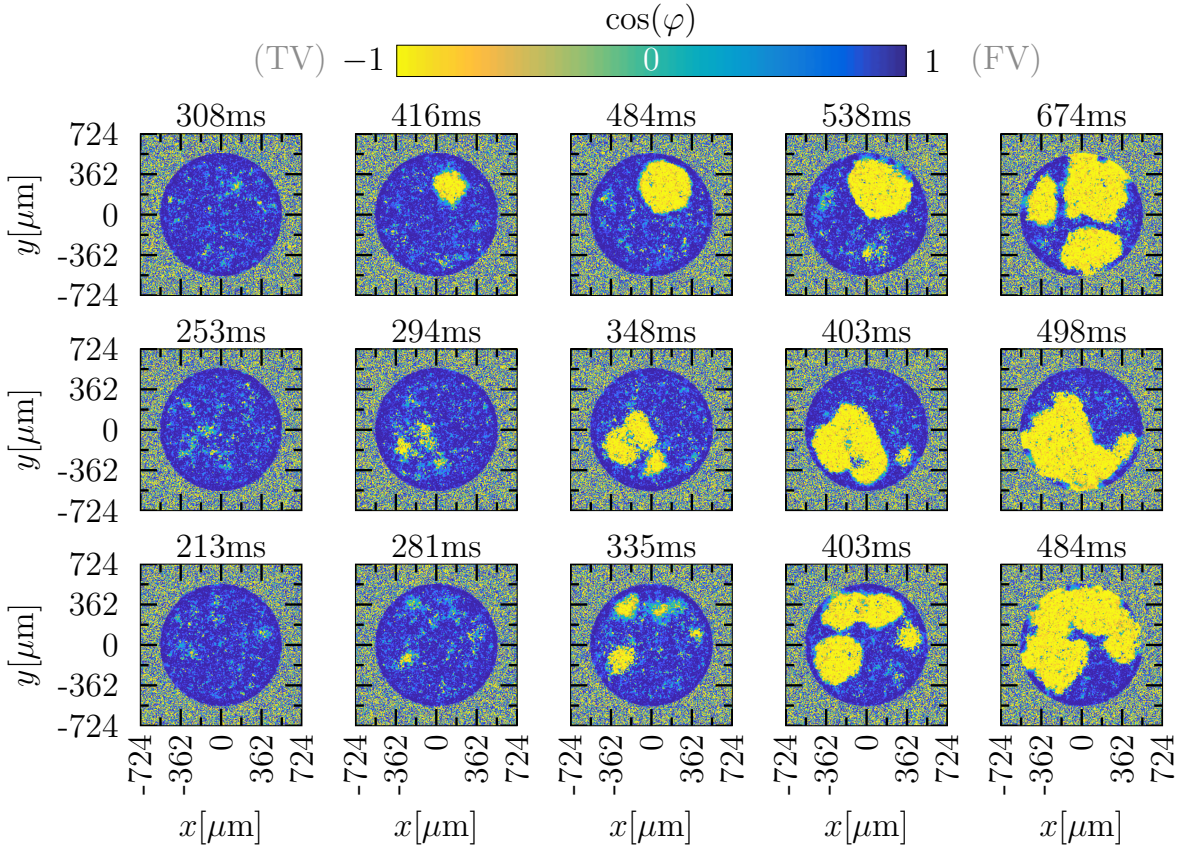


FIG. 8. The evolution of $\cos(\varphi)$ in a spin-1 gas of Rubidium-87 atoms confined to a ‘trench’ potential at $T = 16.56\text{nK}$. Here $r_a = 507\mu\text{m}$, $r_b = 543\mu\text{m}$, and $\sigma = 1.81\mu\text{m}$, with all relevant parameters listed in Table III. Each row of snapshots shows the progression of a unique simulation run, with time increasing from left to right. Identical parameters are used across realizations and all quantities are expressed in physical units.

ACKNOWLEDGEMENTS

This work was supported by the Science and Technology Facilities Council (STFC) [Grant ST/T000708/1] and the UK Quantum Technologies for Fundamental Physics programme [Grants ST/T00584X/1 and ST/W006162/1]. The authors are grateful to Russell Bisset for insightful conversations. This research made use of the Rocket High Performance Computing service at Newcastle University.

TABLE III. Physical parameters used in the rubidium-87 simulations.

Parameter	Value
number density	$n = 100 \mu\text{m}^{-2}$
magnetic field	$B = 0.389\text{G}$
Rabi frequency	$\Omega = 5 \times 2\pi\text{Hz}$
Raman parameter	$\lambda = 1.45$
trap frequency	$\omega_{\perp} = 15 \times 2\pi\text{kHz}$
frequency scale	$\omega_m = 22.1\text{kHz}$
healing length	$\xi_m = 1.81\mu\text{m}$
temperature	$T_m = 55.2\text{nK}$

Appendix A: Bubble wall motion in pseudo-Lorentzian theories

The sodium system is an example where the effective theory is not Lorentz invariant, but bubble wall trajectories are relativistic. We will investigate the motion of bubble walls in such theories by constructing an action for the bubble radius.

The family of theories of interest have Lagrangian density \mathcal{L} of the form

$$\mathcal{L} = \frac{1}{2}F(Z)\dot{Z}^2 - \frac{1}{2}G(Z)(\nabla Z)^2 - V(Z) + V(Z_{FV}) \quad (\text{A1})$$

Lorentz invariance only applies when $G(Z) = c^2F(Z)$, where c is the constant sound speed. This condition will not be imposed. We apply a thin-wall anzatz for the field that extrapolates between the true vacuum value Z_{TV} and the false vacuum value Z_{FV}

$$Z = \frac{1}{2}Z_{TV}(1-f) + \frac{1}{2}Z_{FV}(1+f) \quad (\text{A2})$$

where f depends on two functions, the bubble radius $R(t)$ and a scaling for the wall thickness $\gamma(t)$

$$f = \tanh [\mu\gamma(t)(r - R(t))] \quad (\text{A3})$$

This approach depends on the fact that the action is stationary, and can be approximated with a relatively crude approximation to the field. Due to the thin-wall approximation, we will drop terms with $(1-f^2)(r-R)$ factors. We have

$$\begin{aligned} \dot{Z} &\approx -\frac{\mu\gamma}{2}(1-f^2)\Delta Z \dot{R} \\ Z' &\approx \frac{\mu\gamma}{2}(1-f^2)\Delta Z \end{aligned}$$

where $\Delta Z = Z_{FV} - Z_{TV}$. We also assume a similar anzatz for the potential $V(Z)$, but with an extra term representing the potential barrier around $r = R$, and so we write

$$V = \frac{1}{2}V_{TV}(1-f) + \frac{1}{2}V_{FV}(1+f) + \Delta V(x) \quad (\text{A4})$$

where $x = \mu\gamma(r-R)$.

We define the Lagrangian L in n spatial dimensions by

$$L = \int \mathcal{L} d^n x \quad (\text{A5})$$

After inserting the anzatzes, we arrive at

$$L = \frac{\omega_n}{\mu\gamma} R^{n-1} \left\{ \frac{1}{2} \left(\frac{\mu\gamma}{2} \right)^2 (\Delta Z)^2 c_F \dot{R}^2 - \frac{1}{2} \left(\frac{\mu\gamma}{2} \right)^2 (\Delta Z)^2 c_G - V_B \right\} - \frac{\omega_n}{n} R^n \epsilon \quad (\text{A6})$$

where ω_n is the area of a sphere in n dimensions, $\epsilon = V_{FV} - V_{TV}$, and

$$c_F = \int F(Z)(1-f^2)^2 dx \quad (\text{A7})$$

$$c_G = \int G(Z)(1-f^2)^2 dx \quad (\text{A8})$$

$$V_B = \int \Delta V dx \quad (\text{A9})$$

Now we make a judicious choice of μ to arrange that

$$L = \frac{\omega_n}{2} \sigma \gamma \left(\dot{R}^2/c^2 - 1 - \gamma^{-2} \right) R^{n-1} + \frac{\omega_n}{n} \epsilon R^n \quad (\text{A10})$$

where $c = (c_G/c_F)^{1/2}$ and

$$\mu = \sqrt{\frac{8V_B}{c_G \Delta Z^2}} \quad (\text{A11})$$

$$\sigma = \sqrt{\frac{c_G V_B \Delta Z^2}{2}} \quad (\text{A12})$$

The action should be stationary with respect to variations of γ , which implies

$$\gamma = (1 - \dot{R}^2/c^2)^{-1/2} \quad (\text{A13})$$

We find that the thickness of the bubble is Lorentz contracted, just as in a relativistic theory. Substituting back into the action,

$$L = -\omega_n \sigma (1 - \dot{R}^2/c^2)^{-1/2} R^{n-1} + \frac{\omega_n}{n} \epsilon R^n \quad (\text{A14})$$

The effective theory of the bubble wall is the same as the one we would obtain from a fully Lorentz invariant theory, with propagation speed c and surface tension σ .

- [1] A. Mazumdar and G. White, *Rept. Prog. Phys.* **82**, 076901 (2019), arXiv:1811.01948 [hep-ph].
- [2] M. Hindmarsh, M. Lüben, J. Lumma, and M. Pauly, *SciPost Phys. Lect. Notes*, 24 (2021).
- [3] E. J. Copeland and T. W. B. Kibble, *Proc. Roy. Soc. Lond. A* **466**, 623 (2010), arXiv:0911.1345 [hep-th].
- [4] M. Caneletti and I. G. Moss, *Phys. Rev. D* **110**, 105015 (2024), arXiv:2408.12229 [hep-th].
- [5] M. Hindmarsh, S. J. Huber, K. Rummukainen, and D. J. Weir, *Phys. Rev. Lett.* **112**, 041301 (2014), arXiv:1304.2433 [hep-ph].
- [6] S. R. Coleman, *Phys. Rev. D* **15**, 2929 (1977), [Erratum: *Phys. Rev. D* 16, 1248 (1977)].
- [7] C. G. Callan and S. R. Coleman, *Phys. Rev. D* **16**, 1762 (1977).
- [8] D. Pirvu, J. Braden, and M. C. Johnson, *Phys. Rev. D* **105**, 043510 (2022), arXiv:2109.04496 [hep-th].
- [9] E. Altman, K. R. Brown, G. Carleo, L. D. Carr, E. Demler, C. Chin, B. DeMarco, S. E. Economou, M. A. Eriksson, K.-M. C. Fu, M. Greiner, K. R. Hazzard, R. G. Hulet, A. J. Kollár, B. L. Lev, M. D. Lukin, R. Ma, X. Mi, S. Misra, C. Monroe, K. Murch, Z. Nazario, K.-K. Ni, A. C. Potter, P. Roushan, M. Saffman, M. Schleier-Smith, I. Siddiqi, R. Simmonds, M. Singh, I. Spielman, K. Temme, D. S. Weiss, J. Vučković, V. Vuletić, J. Ye, and M. Zwierlein, *PRX Quantum* **2**, 017003 (2021).
- [10] O. Fialko, B. Opanchuk, A. I. Sidorov, P. D. Drummond, and J. Brand, *EPL (Europhysics Letters)* **110**, 56001 (2015), arXiv:1408.1163 [cond-mat.quant-gas].
- [11] O. Fialko, B. Opanchuk, A. I. Sidorov, P. D. Drummond, and J. Brand, *Journal of Physics B Atomic Molecular Physics* **50**, 024003 (2017), arXiv:1607.01460 [cond-mat.quant-gas].
- [12] J. Braden, M. C. Johnson, H. V. Peiris, and S. Weinfurtner, *JHEP* **07**, 014 (2018), arXiv:1712.02356 [hep-th].
- [13] J. Braden, M. C. Johnson, H. V. Peiris, A. Pontzen, and S. Weinfurtner, *Phys. Rev. Lett.* **123**, 031601 (2019), [Erratum: *Phys. Rev. Lett.* 129, 059901 (2022)], arXiv:1806.06069 [hep-th].
- [14] T. P. Billam, R. Gregory, F. Michel, and I. G. Moss, *Phys. Rev. D* **100**, 065016 (2019), arXiv:1811.09169 [hep-th].
- [15] J. Braden, M. C. Johnson, H. V. Peiris, A. Pontzen, and S. Weinfurtner, *JHEP* **10**, 174 (2019), arXiv:1904.07873 [hep-th].

- [16] K. L. Ng, B. Opanchuk, M. Thenabudu, M. Reid, and P. D. Drummond, *PRX Quantum* **2**, 010350 (2021), arXiv:2010.08665 [quant-ph].
- [17] T. P. Billam, K. Brown, and I. G. Moss, *Phys. Rev. A* **102**, 043324 (2020), arXiv:2006.09820 [cond-mat.quant-gas].
- [18] T. P. Billam, K. Brown, and I. G. Moss, *Phys. Rev. A* **105**, L041301 (2022), arXiv:2108.05740 [cond-mat.quant-gas].
- [19] T. P. Billam, K. Brown, A. J. Groszek, and I. G. Moss, *Phys. Rev. A* **104**, 053309 (2021), arXiv:2104.07428 [cond-mat.quant-gas].
- [20] J. Braden, M. C. Johnson, H. V. Peiris, A. Pontzen, and S. Weinfurtner, (2022), arXiv:2204.11867 [hep-th].
- [21] T. P. Billam, K. Brown, and I. G. Moss, *New Journal of Physics* **25**, 043028 (2023).
- [22] A. C. Jenkins, I. G. Moss, T. P. Billam, Z. Hadzibabic, H. V. Peiris, and A. Pontzen, (2023), arXiv:2311.02156 [cond-mat.quant-gas].
- [23] A. Zenesini, A. Berti, R. Cominotti, C. Rogora, I. G. Moss, T. P. Billam, I. Carusotto, G. Lamporesi, A. Recati, and G. Ferrari, *Nature Physics* **20**, 558 (2024).
- [24] P. Blakie, A. Bradley, M. Davis, R. Ballagh, and C. Gardiner, *Advances in Physics* **57**, 363 (2008), arXiv:0809.1487 [cond-mat.quant-gas].
- [25] A. L. Gaunt, T. F. Schmidutz, I. Gotlibovych, R. P. Smith, and Z. Hadzibabic, *Phys. Rev. Lett.* **110**, 200406 (2013), arXiv:1212.4453 [cond-mat.quant-gas].
- [26] G. Gauthier, I. Lenton, N. M. Parry, M. Baker, M. J. Davis, H. Rubinsztein-Dunlop, and T. W. Neely, *Optica* **3**, 1136 (2016), arXiv:1605.04928 [cond-mat.quant-gas].
- [27] C. W. Gardiner, J. R. Anglin, and T. I. A. Fudge, *Journal of Physics B: Atomic, Molecular and Optical Physics* **35**, 1555 (2002), arXiv:0112129 [cond-mat].
- [28] C. W. Gardiner and M. J. Davis, *Journal of Physics B: Atomic, Molecular and Optical Physics* **36**, 4731 (2003), arXiv:0308044 [cond-mat].
- [29] A. S. Bradley, C. W. Gardiner, and M. J. Davis, *Phys. Rev. A* **77**, 033616 (2008), arXiv:0712.3436 [quant-ph].
- [30] A. S. Bradley and P. B. Blakie, *Phys. Rev. A* **90**, 023631 (2014), arXiv:1406.2029 [cond-mat.quant-gas].
- [31] Y. Kawaguchi and M. Ueda, *Physics Reports* **520**, 253 (2012), arXiv:1001.2072 [cond-mat.quant-gas].
- [32] D. M. Stamper-Kurn and M. Ueda, *Rev. Mod. Phys.* **85**, 1191 (2013), arXiv:1205.1888 [cond-mat.quant-gas].

[mat.quant-gas](#)].

- [33] T. P. Billam, K. Brown, and I. G. Moss, “Data supporting publication: Mitigating boundary effects in finite temperature simulations of falsevacuum decay,” (2025), (Dataset available at doi:10.25405/data.ncl.28194656).